Development of ultrahigh strength and high ductility in nanostructured iron alloys with lattice softening and nanotwins

Edalati, Kaveh
Department of Materials Science and Engineering, Faculty of Engineering, Kyushu University | WPI, International Institute for Carbon-Neutral Energy Research (WPI-I2CNER), Kyushu University

Toh, Shoichi
Research Laboratory for High Voltage Electron Microscopy, Kyushu University

Furuta, Tadahiko
Frontier Research Center, Toyota Central R&D Laboratories Inc.

Kuramoto, Shigeru
Frontier Research Center, Toyota Central R&D Laboratories Inc.

他

出版情報：Scripta Materialia. 67 (5), pp.511-514, 2012-09. Elsevier
バージョン：

Scripta Materialia 67 (2012) 511–514

Received 14 March 2012; Revised 11 June 2012; Accepted 13 June 2012
Available online 21 June 2012

Development of ultrahigh strength and high ductility in nanostructured iron alloys with lattice softening and nanotwins

Kaveh Edalati,[a,b,*] Shoichi Toh,[c] Tadahiko Furuta,[d] Shigeru Kuramoto,[d] Masashi Watanabe[e] and Zenji Horita[a,b]

[a]Department of Materials Science and Engineering, Faculty of Engineering, Kyushu University, Fukuoka 819-0395, Japan
[b]WPI, International Institute for Carbon-Neutral Energy Research (WPI-I2CNER), Kyushu University, Fukuoka 819-0395, Japan
[c]Research Laboratory for High Voltage Electron Microscopy, Kyushu University, Fukuoka 819-0395, Japan
[d]Frontier Research Center, Toyota Central R&D Laboratories Inc., Nagakute, Aichi 480-1192, Japan
[e]Department of Materials Science and Engineering, Lehigh University, Bethlehem, PA 18015, USA

Abstract
Bulk nanostructured materials exhibit high strength but very low ductility. In this study, ductile nanostructured iron-base alloys are successfully developed using a combination of three strategies: appropriate choice of chemical compositions for lattice softening, severe plastic deformation using high-pressure torsion for grain refinement, and annealing for nanotwin formation. Accordingly, exceptional performance of both ultrahigh strength, 2.3–3 GPa, and high elongation to failure, 10–20%, which has never been reported for metallic materials, is achieved.
Keywords: High-pressure torsion (HPT); Martensite; Nanostructure; Ultrafine grain; Twinning.

* Corresponding author at: Department of Materials Science and Engineering, Faculty of Engineering, Kyushu University, Fukuoka 819-0395, Japan. Tel./fax: +81 92 802 2992; e-mail: kaveh.edalati@zaiko6.zaiko.kyushu-u.ac.jp.

The unique physical, chemical and mechanical properties of bulk nanostructured metallic materials make them appropriate for many multifunctional applications [1,2]. However, a general requirement for structural applications is that the materials should have both high strength and high ductility. Although bulk nanostructured metallic materials exhibit very high strength, their ductility is generally low because of limitations in the motion and accumulation of internal lattice defects and lack of strain hardening [3]. Since the introduction of nanostructured materials, several approaches, including severe plastic deformation (SPD) [4–8], twinning [9–14] and lattice softening by composition control [15–18], among others [19,20], have been independently employed for improvement of ductility. In this study, the three approaches mentioned above are combined, and nanostructured Fe–Ni–Co–Ti alloys with ultrahigh tensile strength and high ductility are developed.

Two coarse-grained Fe–Ni–Co–Ti alloys, with compositions, crystal structures and grain sizes as listed in Table 1, were prepared by melting under an Ar atmosphere, subsequent forging at 1423 K and solution treatment at 1373 K for 86.4 ks. In order to produce nanograined structures, disc specimens (10 mm diameter, 0.8 mm thickness) were subjected to SPD by high-pressure torsion (HPT) [21,22] by compression under a pressure of 6 GPa and concurrent rotation of 10 turns at a rotation speed of 0.2 rpm. Following the HPT, phase transformations occurred and a saturation of grain refinement [23] to the levels given in Table 1 was achieved throughout the discs. The HPT-processed samples were subsequently annealed at 473 and 773 K for 3.6 ks to produce nanotwinned structures.

The samples were evaluated by means of Vickers microhardness measurement, X-ray diffraction (XRD) analysis, differential scanning calorimetry (DSC), tensile testing (1.5 mm gauge length, 0.7 mm gauge width and 0.7 mm thickness) and scanning transmission electron microscopy (STEM).

The compositions of these Fe–Ni–Co–Ti alloys were deliberately selected to produce several characteristic features. First, according to first-principles calculations and experimental observations, the alloys exhibit a lattice softening when the average valence electron number per atom (e/a) is about 8.4 [16]. As given in Table 1, the e/a values for the two alloys are close to 8.4. It is noted that a crystal is considered lattice softened when the difference in cubic elastic constants, $C' = (C_{11} - C_{12}) / 2$, is adjusted to be small by controlling the chemical composition [15,16]. As a consequence, the Young's modulus in the <100> direction becomes small and a strong elastic anisotropy and crystal instability is developed. Second, the alloys have different initial crystalline structures before deformation such as γ (austenite) and γ + α' (martensite) phase structures because of the effect of alloying elements on the stability of different phases. Third, the crystal structures of the alloys are unstable when e/a is about 8.4 and the alloys exhibit a strain-induced γ→α' phase transformation. In contrast to α' phase in carbon steels, the α' phase in the present alloys is ductile because of the lattice softening effect [16]. Fourth, the average grain size in these alloys is reduced from ~200 μm to ~20 nm after SPD, whereas the grain size of severely deformed metallic materials is usually larger than 100 nm [24]. Here, the grain refinement is enhanced by lattice softening [16], by combining the phase transformation and plastic deformation [25] and by the twinning effect [11,14]. Fifth, the severely deformed samples exhibit nanotwin formation by subsequent thermal

annealing, and the fraction of nanotwin boundaries increases with increasing annealing temperature. The mechanism of twin formation in the α' phase is not yet fully understood; however, because the energy for twin boundaries, which are known as coherent boundaries, is small [12], the total stored energy should be decreased by twin formation.

Table 1. Characteristics of Fe–Ni–Co–Ti alloys. Chemical composition, average valence electron number per atom (*e*/*a*), crystal structure, average grain size, temperature for elemental distribution (T_e) and temperature for the α' to γ phase transformation (T_γ).

Alloy	Composition, mol.%				*e/a*	Crystal Structure		Average Grain Size		T_e	T_γ
	Fe	Ni	Co	Ti		Before HPT	After HPT	Before HPT	After HPT	(K)	(K)
I	37.6	24.2	32.3	5.9	8.50	γ	γ+α'	210 μm	16 nm	580	702
II	38.4	22.3	34.0	5.3	8.51	γ+α'	α'	140 μm	18 nm	604	694

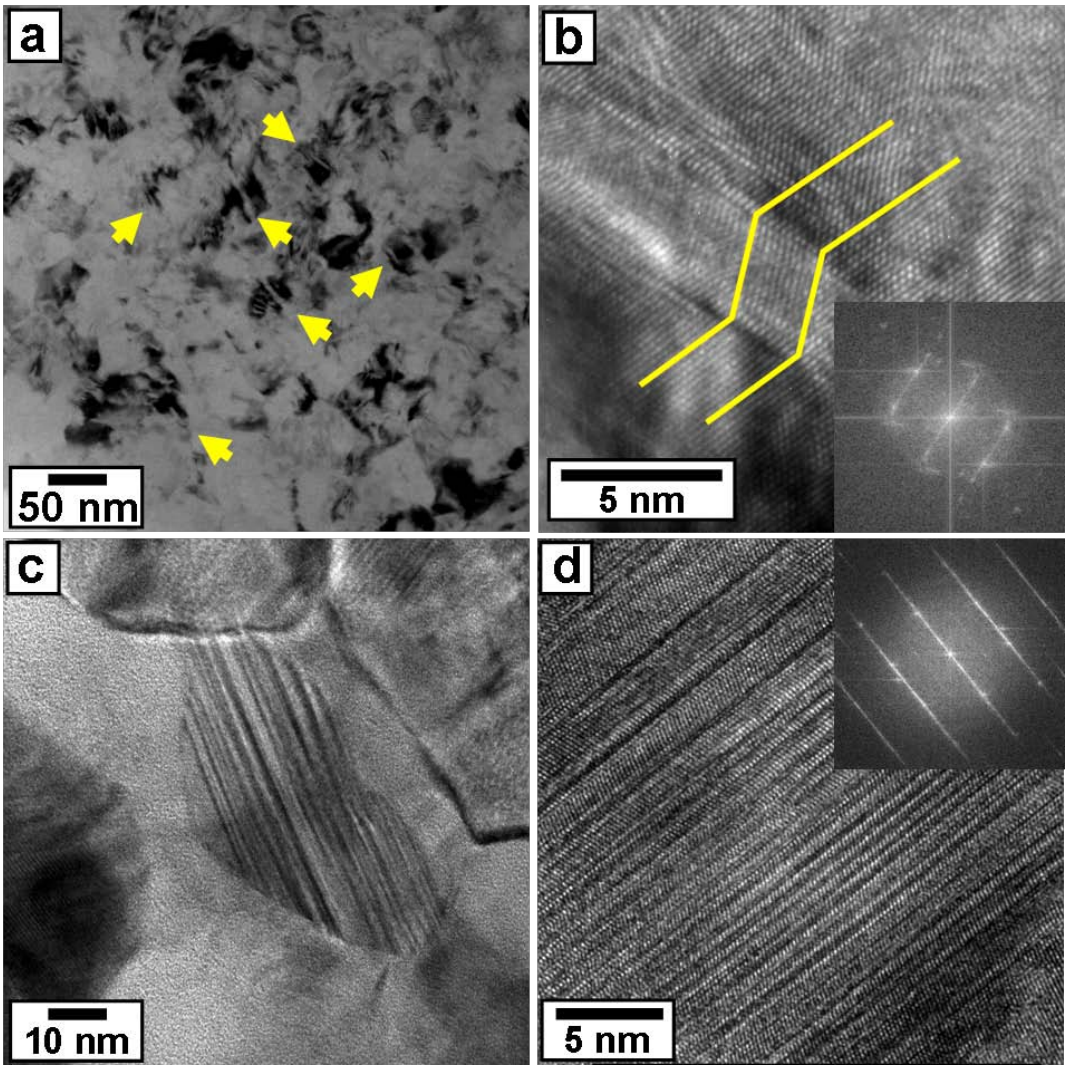

Figure 1. Microstructures of Alloy II after post-HPT annealing at (a and b) 473 K and (c and d) 773 K. (a) TEM bright-field image; (b) lattice image of a twin indicated by an arrow in (a) and corresponding diffractogram; (c) high-resolution image of several grains; and (d) lattice image of one grain and corresponding diffractogram.

Figure 1 shows TEM micrographs of the HPT-processed Alloy II sample after annealing at 473 K (Fig. 1a and b) and 773 K (Fig. 1c and d). Examination of Figure 1 shows that the grains are still retained at the nanometer level but the grain size is slightly increased by annealing at 773 K. Figure 1a shows that there are many nanotwins, as indicated by the arrows, within the nanograins. Since only twins with twin boundaries parallel to the incident electron beam are visible in TEM images, the real twin density should be higher than the one seen in Figure 1a. Close examination of the grains in Figure 1a–d reveals that the width of nanotwins after annealing at 473 K is larger than that after annealing at 773 K. It should be noted that no precipitate formation can be detected after the annealing within the sensitivity limit of the selected-area electron diffraction (SAED) and XRD analyses. However, an elemental distribution is detected by annealing at temperatures above T_e = 580–604 K which results in formation of Ni- and Ti-rich areas. In addition, an α'→γ phase transformation is produced by annealing at temperatures above T_γ = 694–702 K, but the γ phase in both alloys mostly transforms to the α' phase with nanotwins after cooling. As given in Table 1, these temperatures, which were determined from DSC analysis, depend on the compositions of the alloys. The SAED analysis and energy-dispersive X-ray spectrometry (EDS) results, as shown in Figure 2, also confirm that neither elemental distribution nor phase transformation occurs in Alloy II after annealing at 473 K, whereas both elemental distribution and γ-phase formation occur after annealing at 773 K.

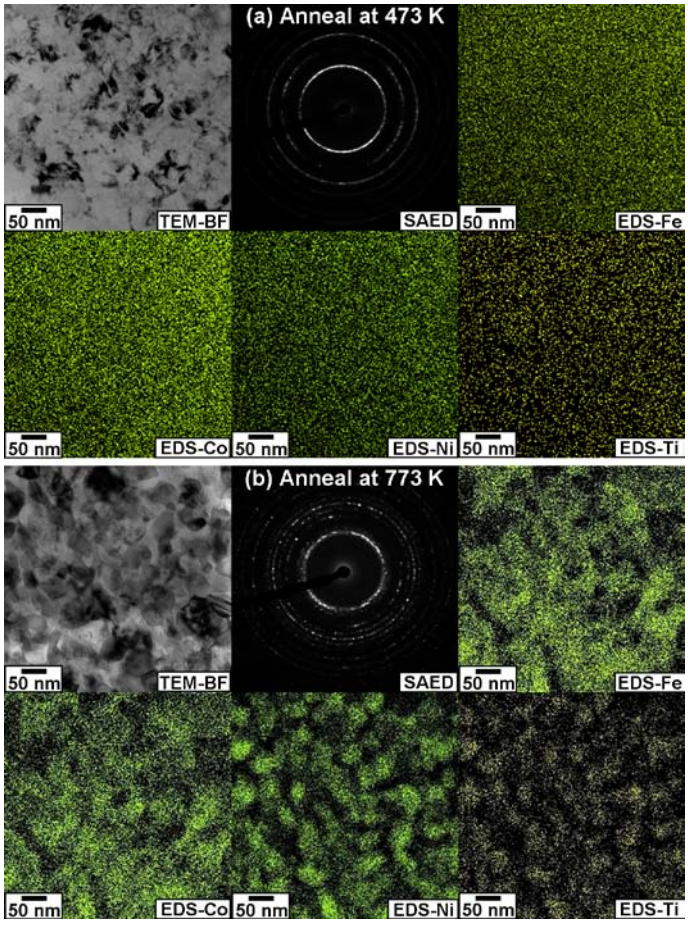

Figure 2. TEM bright-field image, SAED pattern and EDS mappings for Alloy II after post-HPT annealing at (a) 473 K and (b) 773 K.

Figure 3 plots the hardness levels for two alloys with coarse-grained structure produced by solution treatment, nanograined structure produced by HPT processing, and nanotwinned structures produced by post-HPT annealing at 473 K ($T < T_e$) and 773 K ($T > T_\gamma$). The hardness is <4 GPa for the coarse-grained alloys but increases after HPT because of the formation of nanograins. Figure 3 shows that the hardness levels are further enhanced by subsequent annealing due to the formation of nanotwins: this increase is far more significant after annealing at 773 K than at 473 K. For the former, the twin width becomes finer and the fraction of twin boundaries increases, whereas for the latter the width is coarser and the fraction is lower. It is noted that these hardness values are similar to the levels for intermetallics.

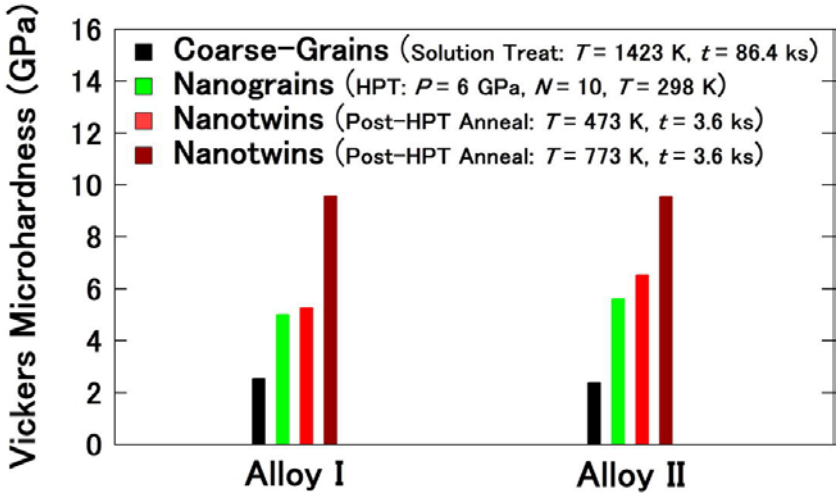

Figure 3. Vickers microhardness of coarse-grained, nanograined and nanotwinned Fe–Ni–Co–Ti alloys.

Some representative stress–strain curves of the two alloys annealed at 473 K ($T < T_e$) are delineated in Figure 4a from tensile testing conducted at room temperature and with an initial strain rate of 2×10^{-3} s^{-1}. The tensile strength is ~2.3 GPa for Alloy I with γ + α' phases, and is higher, ~3 GPa, for Alloy II with α' phase. The elongation to failure is as high as ~20% for Alloy I and ~10% for Alloy II, with a uniform ductility of ~2% for both materials. The difference between the ductility of Alloys I and II should be due to the difference in the fractions of c and a0 phases and the effect of chemical composition on the inherent ductility of the α' and γ phases. It is noted that little ductility was obtained after annealing the two alloys at 773 K ($T > T_\gamma$). The brittle behavior of these alloys after annealing at 773 K is due to the elemental distribution and extremely small width of twins. Since the compositions of these alloys were deliberately selected to produce a lattice softening effect and resultant high ductility, the changes in the composition by the elemental distribution, as shown in Figure 2b, adversely affect the ductility.

The tensile testing results shown in Figure 4a are summarized in Figure 4b in comparison with relevant data including coarse-grained metals produced by high-temperature annealing, nanograined metals produced by HPT, and two amorphous materials produced by casting. Since the dimensions of tensile specimen significantly influence the elongation to failure [26], the tensile properties of

different materials in Figure 4b were measured using tensile specimens of approximately the same size (1–1.5 mm gauge length, 0.7–1 mm gauge width and 0.5–0.7 mm thickness). A solid black line represents the optimum relation between strength and ductility obtained with pure metals. There is a trade-off between the strength and the elongation to failure for all data points plotted in Figure 4b. However, the present Fe–Ni–Co–Ti alloys provide excellent combinations of strength and ductility when compared to other materials.

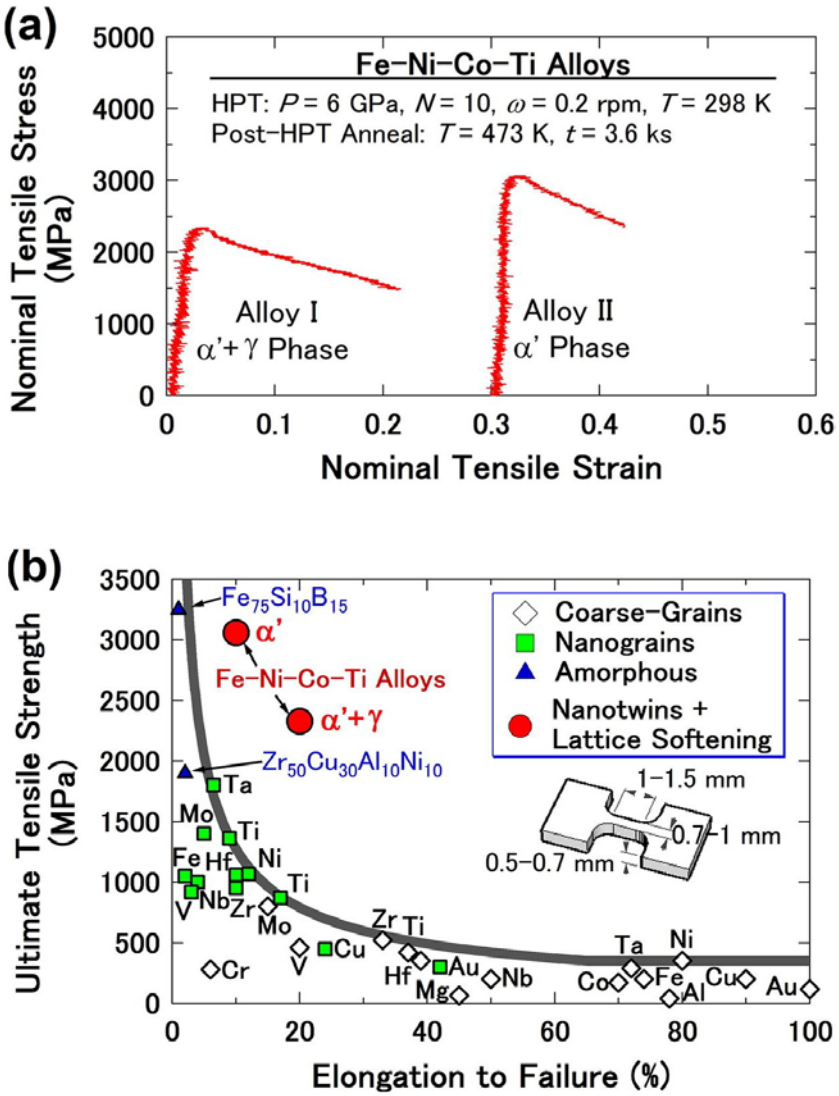

Figure 4. (a) Nominal tensile stress vs. nominal tensile strain curves for post-HPT annealed Fe–Ni–Co–Ti alloys. (b) Ultimate tensile strength vs. elongation to failure for Fe–Ni–Co–Ti alloys including data for coarse-grained metals, nanograined metals and amorphous materials.

A question naturally arises from the current investigation: why are such good combinations of both ultrahigh strength and high ductility achieved in the alloys? The strengthening mechanisms in this study are due to the grain refinement by SPD [4–8], twin formation [9–14] and lattice softening [15–18], although determination of the exact contribution of each mechanism to the mechanical properties requires detailed and quantitative analyses. These mechanisms, as outlined below, are accompanied by a smaller reduction in ductility.

In contrast to conventional plastic deformation methods, SPD produces equiaxed nanograins with high-angle grain boundaries [2]. The high-angle grain boundaries hinder the motion of dislocations and increase the strength of the material. At the same time, the high-angle grain boundaries act as both dislocation sources and sinks so that dislocation accumulation in nanograins and strain hardening becomes difficult. The nanograined materials produced by SPD show ductilities somewhat higher than those produced by other methods [5,6]. It was suggested that the large fraction of non-equilibrium grain boundaries and the high density of lattice point defects enhance the atomic diffusion [27,28] and facilitate other deformation mechanisms such as grain boundary sliding [29,30].

Twin boundaries, which are known as typical coherent boundaries, pin the dislocation motion and increase the strength. Furthermore, the strengthening due to twin boundaries is accompanied by a smaller reduction in ductility because the twin boundaries have a high capacity to generate and accommodate dislocations, and dislocations may transmit twin boundaries or glide along the twin boundaries. Previous investigations on Cu indicated that higher ductility and strength are achieved with a finer width of twins [9,12], but an opposite change in mechanical properties occurs when the twin width is below ~15 nm [31]. It is considered that the low ductility observed in the HPT-processed sample after annealing at 773 K is mainly because of elemental distribution, as shown in Figure 2b. Moreover, the twin width was too small, ~3 nm, to allow dislocations to be generated and be accommodated, and furthermore dislocations hardly move via transmission across the twin boundaries as the nanotwins now completely covered the grains.

Materials with softer lattices exhibit higher ductility; the results of this study are consistent with this relationship. When *C'* is reduced by lattice softening, the ideal shear stress is decreased to a level comparable to the local deformation stress [16] which is expected to result in a reduction in strength. The exact mechanism for the paradox of strengthening via lattice softening is not yet clear. Saito et al. [15] suggested that, because of low ideal shear stress with strong elastic anisotropy, the ideal shear deformation governs the deformation and this dislocation-free plastic deformation mechanism results in the increase in strength. However, a recent study showed that spreading of the core radii of dislocations occurs due to extreme elastic anisotropy and this leads to lower mobility of the dislocations, thereby enhancing the strength [17]. It is also suggested that the extreme elastic anisotropy in lattice-softened materials makes it possible to pin dislocation with fewer lattice obstacles [18].

In summary, ductile nanostructured Fe–Ni–Co–Ti alloys are developed using a combination of three strategies: composition control for lattice softening, SPD for nanograin formation and thermal annealing for nanotwin formation. The current method leads to the simultaneous attainment of ultrahigh strength and high ductility in the nanostructured alloys.

K.E. thanks the Japan Society for Promotion of Science (JSPS) for a postdoctoral scholarship. M.W. acknowledges financial support from National Science Foundation through grant DMR-0804528. This work was supported in part by a Grant-in-Aid for Scientific Research from the

MEXT, Japan, in Innovative Areas “Bulk Nanostructured Metals” and in part by Kyushu University Interdisciplinary Programs in Education and Projects in Research Development.

[1] H. Gleiter, Prog. Mater. Sci. 33 (1989) 223–315.
[2] R.Z. Valiev, R.K. Islamgaliev, I.V. Alexandrov, Prog. Mater. Sci. 45 (2000) 103–189.
[3] M.A. Meyers, A. Mishra, D.J. Benson, Prog. Mater. Sci. 51 (2006) 427–556.
[4] S.X. McFadden, R.S. Mishra, R.Z. Valiev, A.P. Zhilyaev, A.K. Mukherjee, Nature 398 (1999) 684–686.
[5] R.Z. Valiev, I.V. Alexandrov, Y.T. Zhu, T.C. Lowe, J. Mater. Res. 17 (2002) 5–8.
[6] R.Z. Valiev, Nat. Mater. 3 (2004) 511–516.
[7] Y. Wang, M. Chen, F. Zhou, E. Ma, Nature 419 (2002) 912–915.
[8] C.C. Koch, Scripta Mater. 49 (2003) 657–662.
[9] L. Lu, Y.F. Shen, X.H. Chen, L.H. Qian, K. Lu, Science 304 (2004) 422–426.
[10] Y.H. Zhao, J.F. Bingert, X.Z. Liao, B.Z. Cui, K. Han, A.V. Sergueeva, A.K. Mukherjee, R.Z. Valiev, T.G. Langdon, Y.T. Zhu, Adv. Mater. 18 (2006) 2949–2953.
[11] Y.H. Zhao, Y.T. Zhu, X.Z. Liao, Z. Horita, T.G. Langdon, Appl. Phys. Lett. 89 (2006) 121906.
[12] K. Lu, L. Lu, S. Suresh, Science 324 (2009) 349–352.
[13] X. Li, Y. Wei, L. Lu, K. Lu, H. Gao, Nature 464 (2012) 877–880.
[14] Y.T. Zhu, X.Z. Liao, X.L. Wu, Prog. Mater. Sci. 57 (2012) 1–62.
[15] T. Saito, T. Furuta, J.H. Hwang, S. Kuramoto, K. Nishino, N. Suzuki, R. Chen, A. Yamada, K. Ito, Y. Seno, T. Nonaka, H. Ikehata, N. Nagasako, C. Iwamoto, Y. Ikuhara, T. Sakuma, Science 300 (2003) 464–467.
[16] S. Kuramoto, T. Furuta, N. Nagasakko, Z. Horita, Appl. Phys. Lett. 95 (2009) 211901.
[17] D.C. Chrzan, M.P. Sherburne, Y. Hanlumyuang, T. Li, J.W. Morris Jr., Phys. Rev. B 82 (2010) 184202.
[18] T. Li, J.W. Morris Jr., N. Nagasako, S. Kuramoto, D.C. Chrzan, Phys. Rev. Lett. 98 (2007) 105503.
[19] Y. Kimura, T. Inoue, F. Yin, K. Tsuzaki, Science 320 (2008) 1057–1060.
[20] R.O. Ritchie, Nat. Mater. 10 (2011) 817–822.
[21] R.Z. Valiev, Y. Estrin, Z. Horita, T.G. Langdon, M.J. Zehetbauer, Y.T. Zhu, JOM 58 (4) (2006) 33–39.
[22] A.P. Zhilyaev, T.G. Langdon, Prog. Mater. Sci. 53 (2008) 893–979.
[23] R. Pippan, S. Scheriau, A. Taylor, M. Hafok, A. Hohenwarter, A. Bachmaier, Annu. Rev. Mater. Res. 40 (2010) 319–343.
[24] K. Edalati, Z. Horita, Acta Mater. 59 (2011) 6831–6836.
[25] N. Tsuji, T. Maki, Scripta Mater. 60 (2009) 1044–1049.
[26] Y.H. Zhao, Y.Z. Guo, Q. Wei, A.M. Dangelewicz, C. Xu, Y.T. Zhu, T.G. Langdon, Y.Z. Zhou, E.J. Lavernia, Scripta Mater. 59 (2008) 627–630.
[27] T. Fujita, Z. Horita, T.G. Langdon, Philos. Mag. A 82 (2002) 2249–2262.
[28] S.V. Divinski, J. Ribbe, D. Baither, G. Schmitz, G. Reglitz, H. Rosner, K. Sato, Y. Estrin, G. Wilde, Acta Mater. 57 (2009) 5706–5717.
[29] R.Z. Valiev, E.V. Kozlov, Y.F. Ivanov, J. Lian, A.A. Nazarov, B. Baudelet, Acta Metall. Mater. 42 (1994) 2467–2475.
[30] N.Q. Chinh, P. Szommer, Z. Horita, T.G. Langdon, Adv. Mater. 18 (2006) 34–39.
[31] L. Lu, X. Chen, X. Huang, K. Lu, Science 323 (2009) 607–610.